TECHNICAL MEMORANDUMS

NATIONAL ADVISORY COMMITTEE FOR AERONAUTICS

No. 1011

PRESSURE DISTRIBUTION ON WINGS IN REVERSED FLOW

By A. Naumann

Jahrbuch 1938 der Deutschen Luftfahrtforschung

Washington
April 1942

NATIONAL ADVISORY COMMITTEE FOR AERONAUTICS

TECHNICAL MEMORANDUM NO. 1011

PRESSURE DISTRIBUTION ON WINGS IN REVERSED FLOW*

By A. Naumann

SUMMARY

The series of pressure distribution measurements at three test sections on NACA airfoils 2212 and M6 within 170° to 210° angles of attack in reversed flow proved to be largely independent of the profile form. In contradiction to the pressure distribution in normal flow considerable negative pressure from the upper surface spills over onto the lower surface, and vice versa, even in the zone of sound flow. The results are presented as chordwise pressure and load distribution. The spanwise lift distribution and the total lift coefficients of the wing obtained by integration manifest approximate agreement with the behavior of a diagonally disposed flat plate. By consideration of the ground effect (represented by a flat wall) the lower surface of the wing shows an increase in the low pressure.

INTRODUCTION

It is known from experience that the movable surfaces of an aircraft tethered in the open are subjected to severe moments in a tail wind. In order to obtain some data regarding the magnitude of these moments and of the load distribution in reversed flow, a series of pressure distributions were carried out which, in the interest of widest possible applicability of the results, were for the time being limited to wings without movable surfaces. Experiments of similar nature are not available, as far as is known.

TEST PROCEDURE AND EXECUTION

The tests were made on an airfoil of medium camber (NACA 2212) and on one with slight reverse camber (NACA M6).

*"Druckverteilung an Flügeln bei Anströmung von rückwärts." Jahrbuch 1938 der deutschen Luftfahrtforschung, pp. I 90–I 100.

Both were rectangular in plan form, had an aspect ratio of 1:5 and 1 meter span. The pressure distribution was recorded at wing center (test section I), at 1.4 chord distance from wing center (test section II) and at 0.1 chord distance from the wing tip (test section III) (fig. 1). Each of these three sections was provided with 26 pressure taps of 0.75 millimeter diameter (fig. 2) located in profile sections made of brass of 10 and 12 millimeters width respectively. The rest of the wing was made of wood. Table 1 gives the spacing of the test orifices measured in millimeters and percent of chord from wing trailing edge along the chord. Each pressure orifice was fitted with brass tubing for conveying the pressure. The pressure lines to the manometers passed through the wing and emerged at the two tips.

Because this arrangement had falsified the measurement in test section III closest to the tip and for reasons of easier fabrication of the models, only sections I and II were first fitted. For the measurement in III the wing was cut at 0.1 chord distance from test section I and this section used as free wing tip. These measurements were therefore made with a wing of approximately half span. The other half of the wing was formed by a straight wall set at right angles to this wing half parallel to the flow direction and this was very large compared to the wing dimensions (fig. 3). The minor discrepancies due to the slightly modified wing aspect ratio and the effect of the boundary layer at the wall were disregarded.

The pressure measurements were made at geometric angles of attack $\alpha' = 170^\circ$, 180°, 190°, 200°, and 210°; 170° denotes reversed flow from below, 190°, 200°, and 210° reversed flow from above. Allowing for the angle of attack correction due to the finite air stream dimensions the true flow angles are $\alpha = 170.4^\circ$, 180°, 189.7°, 199.7°, and 209.7° (cf. section IV).

In several cases the pressure distribution was also measured under ground effect. Since this effect at small distance between wing and ground (low-wing monoplane) and at great angle of attack was expected to be very pronounced, these measurements were made at angle of attack approaching α_{max} (referred to normal setting) and at a distance of 0.6 chord from the leading edge (fig. 4). A lift measurement in the normal angle-of-attack range gave $\alpha_{max} = 20^\circ$ for NACA airfoil 2212 (as against $\alpha = 200^\circ$ in reversed flow at this setting), and $\alpha_{max} = 18^\circ$ for M6 (corresponding to $\alpha = 198^\circ$).

Since the flow is already separated on the lower surface at these settings in reversed flow the overstepping of α_{max} was not anticipated to disclose anything unusual in pressure distribution. For the ground effect measurements the angles on the NACA 2212 were $\alpha' = 194°$, $198°$, $202°$, that on the M6 $\alpha' = 198°$. The flow angles after correction of angle of attack were $\alpha = 193.6°$, $197.6°$, and $201.7°$. The ground was simulated by a flat wooden wall. The dynamic pressure throughout the tests was $q = 56$ millimeters water column, equivalent to a speed of around 30 meters per second. A check test at $q = 39.1$ millimeters water column (25 m/s) with dimensionless values showed the same results. Several Prandtl type micromanometers with vertical tube served as pressure instruments.

RESULTS

The test values made nondimensional by $q = 56$ millimeters water column are given in tables 2 and 3 for the NACA airfoil sections 2212 and M6, respectively, and table 4 gives the results with ground effect. In figures 5 to 12 (NACA airfoil section 2212) and 13 to 18 (M6) the recorded pressure differences are shown plotted against the wing chord referred to atmospheric pressure (p/q). The included airfoil facilitates the identification of the pressure at the different stations. Test sections I, II, and III are marked individually; whereas the p/q values of the upper surface (test stations 1 to 15) are shown as a solid curve and those of the lower surface as dashed curves.

Qualitatively, there is no difference in pressure distribution between the two airfoil sections, both showing a predominant low pressure on the upper surface at $\alpha = 170°$, and positive pressure at 2/3 of the lower surface. The low-pressure region extends over the nose far over the bottom surface. On the contrary, the high-pressure zone of the upper surface extends only to about half the wing chord at $\alpha = 190°$. At $\alpha = 180°$ upper and lower surface have approximately the same pressure distribution, the low pressure at the upper surface being slightly predominant, so that a slight lift occurs. This resultant lift is greater on the M6 than on the NACA 2212. The constancy of the low pressure on the lower surface at $\alpha = 200°$ and $210°$ is indicative of already separated flow at the edge; the profile has approximately the same effect as an obliquely disposed flat plate.

Test sections I and II (that is, those located at midsection) show qualitatively and approximately, also quantitatively the same distribution. At the settings where the flow on the lower surface has separated, the difference at test station II is, of course, greater than at station I. In the pressure variation at the section near the wing tip the pressure equalization over the tips makes itself felt in a substantially lower pressure difference between upper and lower surface, the settings of the separated state of flow again forming an exception. Rather unusual is the marked low-pressure peak on the upper surface at $\alpha = 170^\circ$, on the lower surface in test section III at 190°. But this region of marked low-pressure is restricted to small depth. This is probably a case of edge angle effect as known from flow around a sharp edge.

A lucid picture of the pressure distribution along the wing is afforded when the pressure p/q recorded at the different orifices is plotted at right angles to the profile contour as exemplified on the NACA airfoil 2212 at $\alpha = 170.4^\circ$ in figure 19, and at $\alpha = 189.7^\circ$ in figure 20. The arrows pointing toward the profile indicate positive pressure, those away from it low pressure, the double arrow shows the flow direction. The low pressure region of the lee side extends far over the weather side; the positive pressure zone of the lower surface at $\alpha = 170^\circ$ and of the upper surface at $\alpha = 190^\circ$ is comparatively small. The stagnation point is very close to the trailing edge; its position is indicated by dashed arrow. Since the method of presentation of figures 19 and 20 appears only of interest for the design of ribs, which, on the other hand, does not ordinarily follow the present case of reversed flow, the reproduction of the other measurements in this form is omitted.

The spanwise load distribution is illustrated in figures 21a to 21h for NACA airfoil section 2212 as the sum of the chordwise pressure forces of upper and lower surface against the chord. Figures 22a to 22f show that for airfoil M6. The flow is from left to right throughout. These graphs also confirm the extended agreement of the results at both airfoils. They also disclose the difference in distribution at midsection and the edge, which can become of importance especially in view of compensations.

Ground effect.- The several measurements with ground (figs. 10 to 12, and 18, 21f to 21h and 22f) all disclosed a more marked low pressure at the lower surface than for

the same angle settings without ground, which corresponds to a greater resultant aerodynamic force. The reason for it is likely to be found in the enhanced speed of flow at the lower surface. Qualitatively the pressure distributions with ground do not differ from those recorded without it, by reason of the separation of flow at the lower surfaces on both. On the M6 a pronounced low pressure peak occurs on test section II of the lower surface for $\alpha = 197.7^{\circ}$, the influence of which persists even at the edge. Other measurements showed no similar peaks.

LIFT DISTRIBUTION

Integration of the pressure distributions plotted against chord affords the normal force coefficient

$$c_n = \oint \frac{p}{q} \, d\left(\frac{x}{t}\right)$$

and similarly the coefficient of the tangential force

$$c_t = \oint \frac{p}{q} \, d\left(\frac{y}{t}\right)$$

From c_t and c_n follows the local lift coefficient

$$c_a = c_n \cos \alpha - c_t \sin \alpha$$

Since c_t is small, $c_a = c_n \cos \alpha$.

In view of the measurements with ground c_a was consistently figured positive when the low pressure on the top camber predominates, that is, when c_n is positive (in a body-axis system), which, applied to measurements with ground means that the positive c_a direction points away from the ground (fig. 4). This definition which results when the wind direction about the fixed wing is rotated and the air forces described in a system of space axes differs from the conventional in the sign of c_a in the second and third quadrant. More precisely,

$$c_a = c_n |\cos \alpha|$$

the c_n on NACA airfoil 2212 was determined at sections I, II, and III; and at $\alpha = 199.7^{\circ}$, that is, where the

flow has separated; hence a high drag anticipated, c_t was also measured. It was found that in the separated zone also $c_t \sin \alpha$ can be disregarded with respect to $c_n \cos \alpha$. So the time-consuming integration of c_t was omitted and $c_a = c_n \cos \alpha$ considered only, and affording in this manner the lift distribution over the span 2 x/b (fig. 23). The values of the right half of the wing are reflected on the left half in figure 23; whereas in figure 24 the local c_a for the individual test stations are plotted separately against the angle of attack. The integration of the c_a distribution curves over the span give the c_a value for the total wing which is also shown in figure 24 plotted against the angle of attack.

With this c_a curve as a basis the final angle of attack correction due to the finite jet diameter was applied. This correction amounts to 0.4° at the highest. In view of the accord of the pressure distributions on both airfoils the corrections were ascertained on the airfoil 2212 only and the same correction factors applied to the M6. Numerically the values are given in table 5.

The graphs confirm the fact mentioned that the flow within 170° to 190° is not substantially separated, but completely so at α = 200° and 210°. At the edge (test section III) the separation at the lower surface starts at about α = 198°, on the two midsections I and II at around α = 191°.

Comparison with Göttingen test data on flat rectangular plates of 5:1 aspect ratio (reference 1) showed good agreement of the c_a values, particularly also the position and approximately the amount of $c_{a_{max}}$. An estimation of the c_t values from our measurements also gives a close accord for the c_w values as to the order of magnitude. It is suspected that the obliquely disposed wing in reversed flow largely approaches in its attitude of flow that of a flat rectangular plate. The Göttingen airfoil section 420 (reference 2) measured in the total angle-of-attack range itself has c_a and c_w values in the vicinity of 180°, which, in regard to order of magnitude, are in good agreement with the present findings.

Figure 25 shows the c_a value for the flat rectangular plate, airfoil section 420 and airfoil section 2212.

The three measurements with ground on airfoil 2212 give, in accord with the increased low pressure of the lower surface, greater c_a values without ground. Figure 25 represents the lift distribution of the measurements under ground effect. The lateral $c_{a_{min}}$ here reach higher values than in the measurements without ground. The c_a values obtained by integration of the spanwise lift distribution likewise afford higher (negative) values than without ground; the ground proximity induces a supplementary force directed toward the ground. Table 6 contains the results of the evaluation.

Translation by J. Vanier,
National Advisory Committee
for Aeronautics.

REFERENCES

1. Flachsbart, O.: Messungen an ebenen und gewölbten Platten. Ergb. d. Aerodyn. Versuchsanstalt zu Göttingen, IV Lfg., R. Oldenbourg (München and Berlin) 1932, p. 96.

2. Messung eines Profils bei Anstellwinkeln von 0 bis 360°. Ergb. d. Aerodyn. Versuchsanstalt zu Göttingen, III Lfg., R. Oldenbourg (München and Berlin) 1927, p. 78.

Table I.- Location of the test stations at both profiles.

Test station		1	2	3	4	5	6	7	8	9	10	11	12	13
Distance from wing trailing edge	mm	0	5,25	11,25	17,25	23,5	30	51	78	110	137	158	178	188
	$\%_0 t$	0	0,0263	0,0563	0,0862	0,117	0,150	0,255	0,390	0,550	0,685	0,790	0,890	0,940

Test station		14	15	16	17	18	19	20	21	22	23	24	25	26
Distance from wing trailing edge	mm	196	200	191	182	167	145	120	90	61	36,5	21,0	14,75	8,5
	$\%_0 t$	0,980	1,00	0,954	0,910	0,835	0,725	0,600	0,450	0,305	0,182	0,105	0,0737	0,0425

Table V.- Normal force and lift coefficients, NACA airfoil 2212.

α'	c_n			$c_a = c_n \cos\alpha$				$\Delta\alpha$	α
	I	II	III	I	II	III	$c_{a\,\mathrm{mes}}$		
170°	0,83	0,82	0,47	0,82	0,81	0,46	0,75	0,38	170,4
180°	0,11	0,063	—	0,11	0,063	—	0,085	0,033	180
190°	−0,68	−0,70	−0,45	−0,67	−0,69	−0,44	−0,62	0,31	189,7
200°	−0,54	−0,67	−0,71	−0,51	−0,63	−0,67	−0,60	0,30	199,7
210°	−0,63	−0,73	−0,69	−0,55	−0,63	−0,60	−0,61	0,31	209,7

Table VI.- Normal force and lift coefficients, NACA airfoil 2212 with ground.

α'	c_n			$c_a = c_n \cos\alpha$				$\Delta\alpha$	α
	I	II	III	I	II	III	$c_{a\,\mathrm{mes}}$		
194	−0,67	−0,80	−0,63	−0,66	−0,77	−0,62	−0,71	0,36	193,7
198	−0,64	−0,87	−0,66	−0,61	−0,83	−0,63	−0,74	0,37	197,6
202	−0,60	−0,76	−0,83	−0,56	−0,71	−0,77	−0,67	0,34	201,7

Table II.
Pressure distribution measurement.

Profile NACA 2212 $q = 56$ kg/m²

Test station	$\alpha = 170{,}4^0$			$\alpha = 180^0$			$\alpha = 189{,}7^0$			$\alpha = 199{,}7^0$			$\alpha = 209{,}7^0$		
	I	II	III	I	II	III	I	II	III	I	II	III	I	II	III
1	−0,853	+0,024	+0,378	+0,700	+0,985	+0,997	−0,402	−0,361	−0,283	−0,452	−0,612	−0,760	−0,379	−0,525	−0,620
2	−1,001	−0,939	−1,352	+0,181	+0,272	+0,190	+0,882	+0,881	+0,703	+0,980	+0,982	+0,839	+1,010	+1,000	+0,867
3	−1,013	−0,887	−1,118	+0,0803	+0,188	+0,136	+0,738	+0,570	+0,545	+0,880	+0,680	+0,700	+0,985	+0,803	+0,805
4	−1,030	−0,960	−0,559	+0,0379	+0,139	+0,108	+0,642	+0,630	+0,436	+0,795	+0,794	+0,593	+0,935	+0,924	+0,711
5	−1,038	−0,961	−0,238	+0,0116	+0,097	+0,0745	+0,564	+0,540	+0,350	+0,725	+0,697	+0,500	+0,873	+0,833	+0,626
6	−1,088	−0,976	−0,212	+0,0073	+0,0533	+0,0365	+0,496	+0,482	+0,286	+0,655	+0,651	+0,424	+0,825	+0,806	+0,558
7	−1,052	−1,000	−0,267	−0,0991	−0,054	−0,0438	+0,314	+0,296	+0,136	+0,464	+0,442	+0,261	+0,646	+0,616	+0,363
8	−0,907	−0,911	−0,302	−0,214	−0,171	−0,122	+0,113	+0,102	+0,0131	+0,228	+0,212	+0,0774	+0,416	+0,381	+0,184
9	−0,614	−0,640	−0,334	−0,294	−0,257	−0,177	−0,070	−0,0555	−0,0985	−0,0165	−0,0394	−0,0715	+0,158	+0,117	−0,0013
10	−0,416	−0,434	−0,411	−0,378	−0,331	−0,263	−0,242	−0,212	−0,220	−0,255	−0,311	−0,228	−0,114	−0,184	−0,234
11	−0,322	−0,326	−0,480	−0,432	−0,424	−0,307	−0,334	−0,277	−0,294	−0,426	−0,536	−0,340	−0,340	−0,453	−0,439
12	−0,263	−0,255	−0,665	−0,402	−0,283	−0,343	−0,280	−0,210	−0,292	−0,434	−0,623	−0,415	−0,470	−0,659	−0,725
13	−0,234	−0,223	−0,737	−0,220	−0,227	−0,189	−0,276	−0,213	−0,293	−0,404	−0,574	−0,372	−0,413	−0,584	−0,666
14	−0,188	−0,220	−0,435	−0,1092	−0,160	+0,0073	−0,297	−0,212	−0,314	−0,423	−0,530	−0,390	−0,407	−0,564	−0,633
15	−0,194	−0,175	−0,296	−0,0803	−0,114	+0,0365	−0,290	−0,206	−0,340	−0,421	−0,547	−0,429	−0,392	−0,554	−0,648
16	−0,215	−0,178	−0,229	−0,265	−0,330	−0,177	−0,364	−0,235	−0,645	−0,440	−0,597	−0,550	−0,397	−0,582	−0,686
17	−0,222	−0,205	−0,222	−0,254	−0,319	−0,197	−0,383	−0,262	−0,515	−0,454	−0,614	−0,514	−0,421	−0,577	−0,663
18	−0,141	−0,172	−0,151	−0,196	−0,266	−0,156	−0,427	−0,327	−0,365	−0,458	−0,641	−0,505	−0,424	−0,601	−0,675
19	−0,0517	−0,0655	−0,104	−0,193	−0,227	−0,131	−0,520	−0,438	−0,286	−0,456	−0,636	−0,533	−0,424	−0,598	−0,686
20	+0,0438	+0,0292	−0,073	−0,166	−0,212	−0,125	−0,628	−0,594	−0,276	−0,453	−0,634	−0,630	−0,420	−0,593	−0,676
21	+0,1605	+0,147	−0,0073	−0,125	−0,153	−0,098	−0,725	−0,777	−0,272	−0,441	−0,623	−0,817	−0,414	−0,569	−0,673
22	+0,306	+0,296	+0,0773	−0,0482	−0,0868	−0,0555	−0,750	−0,856	−0,266	−0,426	−0,605	−0,885	−0,409	−0,554	−0,643
23	+0,458	+0,448	+0,200	+0,00584	−0,0292	−0,00876	−0,726	−0,845	−0,227	−0,410	−0,592	−0,826	−0,401	−0,550	−0,615
24	+0,604	+0,580	+0,324	+0,0497	+0,0128	+0,0234	−0,712	−0,823	−0,640	−0,405	−0,586	−0,785	−0,387	−0,543	−0,605
25	+0,689	+0,662	+0,403	+0,0584	+0,0197	+0,0278	−0,716	−0,817	−1,660	−0,403	−0,586	−0,774	−0,389	−0,537	−0,622
26	+0,785	+0,747	+0,516	+0,1092	+0,0285	+0,0263	−0,706	−0,797	−1,850	−0,398	−0,599	−0,765	−0,390	−0,538	−0,621

Table III.
Pressure distribution measurement.

Profile M 6 $q = 56$ kg/m²

Test station	$\alpha = 170{,}4°$			$\alpha = 180°$			$\alpha = 189{,}7°$			$\alpha = 199{,}7°$			$\alpha = 209{,}7°$		
	I	II	III	I	II	III	I	II	III	I	II	III	I	II	III
1	− 0,360	− 0,547	+ 0,270	+ 0,985	+ 1,009	+ 0,99	− 0,255	− 0,382	− 0.0342	− 0,543	− 0,699	− 0,464	− 0,416	− 0,517	− 0,611
2	− 1,18	− 1,122	− 1,94	+ 0.175	+ 0,218	+ 0,146	+ 0,900	+ 0,890	+ 0,690	+ 0,989	+ 0,992	+ 0,834	+ 1,010	+ 1,010	+ 0,864
3	− 1,182	− 1.140	− 1,50	+ 0,128	+ 0,153	+ 0,093	+ 0,745	+ 0,726	+ 0,520	+ 0,887	+ 0,876	+ 0,691	+ 0,990	+ 0,983	+ 0,787
4	− 1,195	− 1,135	− 0,124	+ 0,0960	+ 0,111	+ 0,070	+ 0,646	+ 0,600	+ 0,406	+ 0,800	+ 0,778	+ 0,722	+ 0,941	+ 0,889	+ 0,687
5	− 1,182	− 1,175	− 0,159	+ 0,0684	+ 0,083	+ 0,057	+ 0,576	+ 0,561	+ 0,322	+ 0,728	+ 0,722	+ 0,498	+ 0,887	+ 0,871	+ 0,615
6	− 1,22	− 1,190	− 0,202	+ 0,0378	+ 0,0596	+ 0,0386	+ 0,516	+ 0,505	+ 0,268	+ 0,670	+ 0,662	+ 0,433	+ 0,838	+ 0,817	+ 0,553
7	− 1,175	− 1.115	− 0,228	+ 0,0146	− 0,0436	− 0,0306	+ 0,340	+ 0,330	+ 0,150	+ 0,482	+ 0,471	+ 0,257	+ 0,678	+ 0,657	+ 0,374
8	− 0,756	− 0.633	− 0,302	− 0,226	− 0.203	− 0,134	+ 0,121	+ 0,117	+ 0,0004	+ 0.230	+ 0,220	+ 0,080	+ 0,438	+ 0,413	+ 0,188
9	− 0,432	− 0.422	− 0,399	− 0,417	− 0,415	− 0,258	− 0,144	− 0,153	− 0,150	− 0,0902	− 0,125	− 0,116	+ 0,108	+ 0,0656	− 0,0368
10	− 0,386	− 0.442	− 0,485	− 0,546	− 0,533.	− 0,356	− 0,343	− 0,334	− 0,281	− 0,367	− 0,425	− 0,309	− 0,208	− 0,266	− 0,319
11	− 0,317	− 0,376	− 0.521	− 0,545	− 0.510	− 0.382	− 0,391	− 0,360	− 0,328	− 0,505	− 0,593	− 0,390	− 0,419	− 0,484	− 0,498
12	− 0,192	− 0.236	− 0,586	− 0,423	− 0,405	− 0,354	− 0,310	− 0,284	− 0,254	− 0,447	− 0,602	− 0,403	− 0,502	− 0,612	− 0,687
13	− 0.141	− 0.144	− 0,634	− 0,192	− 0,153	− 0,248	− 0,316	− 0,296	− 0,301	− 0,432	− 0,572	− 0,364	− 0,429	− 0,557	− 0,701
14	− 0,112	− 0,0093	− 0,488	+ 0,0058	− 0,0196	− 0,0292	− 0,269	− 0,207	− 0,228	− 0,438	− 0,543	− 0,381	− 0,417	− 0,562	− 0,650
15	− 0,093	− 0,072	− 0,222	+ 0,0248	+ 0,0051	+ 0.0211	− 0,241	− 0,174	− 0,338	− 0,428	− 0,535	− 0,388	− 0,425	− 0,540	− 0,640
16	− 0.0975	− 0,077	− 0,180	− 0,116	− 0,204	− 0.0860	− 0,282	− 0,216	− 0,446	− 0,443	− 0,603	− 0,432	− 0,425	− 0,553	− 0,690
17	− 0,138	− 0,115	− 0,212	− 0,151	− 0,214	− 0,1165	− 0,314	− 0,237	− 0,388	− 0,454	− 0,627	− 0,445	− 0,438	− 0,572	− 0,689
18	− 0,0545	− 0.0437	− 0,134	− 0,115	− 0,134	− 0,0865	− 0,372	− 0,305	− 0,245	− 0,456	− 0,645	− 0,463	− 0,442	− 0,575	− 0,689
19	+ 0,0247	+ 0,0291	− 0,0672	− 0,074	− 0,099	− 0,0620	− 0,473	− 0,415	− 0,195	− 0,458	− 0,643	− 0,527	− 0,451	− 0,587	− 0,700
20	+ 0,067	+ 0,0581	− 0,0600	− 0,0945	− 0,125	− 0,0765	− 0,594	− 0,561	− 0,216	− 0,453	− 0,632	− 0,627	− 0,450	− 0,566	− 0,689
21	+ 0,142	+ 0,125	− 0,0219	− 0,105	− 0,127	− 0 0815	− 0,727	− 0,729	− 0,245	− 0,455	− 0,608	− 0,758	− 0,438	− 0,566	− 0,677
22	+ 0,236	+ 0,217	+ 0,0365	− 0,109	− 0,131	− 0,0845	− 0,810	− 0,840	− 0,306	− 0,432	− 0,593	− 0,811	− 0,433	− 0,537	− 0,660
23	+ 0,375	+ 0,354	+ 0,129	− 0,090	− 0,115	− 0,077	− 0,810	− 0,861	− 0,342	− 0,418	− 0,582	− 0,775	− 0,422	− 0,530	− 0,615
24	+ 0,545	+ 0,523	+ 0,276	− 0,0276	− 0,051	− 0,0277	− 0,795	− 0,838	− 0,266	− 0,412	− 0,587	− 0,738	− 0,419	− 0,534	− 0,617
25	+ 0,638	+ 0,628	+ 0,383	+ 0,0218	+ 0,00109	+ 0,0124	− 0,793	− 0,837	− 1,11	− 0,413	− 0,596	− 0,735	− 0,415	− 0,520	− 0,597
26	+ 0,770	+ 0,760	+ 0,535	+ 0,0350	+ 0,0764	+ 0,070	− 0,782	− 0,863	− 1,81	− 0,412	− 0,618	− 0,710	− 0,413	− 0,525	− 0,601

Table IV.
Pressure distribution measurement with ground.

Test station	Profile NACA 2212									Profile M 6		
	$\alpha = 193{,}7°$			$\alpha = 197{,}6°$			$\alpha = 201{,}7°$			$\alpha = 197{,}6°$		
	I	II	III	I	II	III	I	II	III	I	II	III
1	−0,405	−0,750	−0,800	−0,714	−0,906	−0,915	−0,781	−0,777	−1,161	−0,354	−1,86	−0,682
2	+0,874	+0,907	+0,745	+0,899	+0,938	+0,760	+0,937	+0,960	+0,824	+0,920	+0,966	+0,781
3	+0,729	+0,591	+0,570	+0,771	+0,637	+0,600	+0,819	+0,724	+0,685	+0,777	+0,816	+0,599
4	+0,634	+0,659	+0,445	+0,681	+0,714	+0,473	+0,737	+0,757	+0,572	+0,687	+0,727	+0,461
5	+0,560	+0,562	+0,352	+0,598	+0,610	+0,371	+0,664	+0,671	+0,469	+0,612	+0,646	+0,380
6	+0,485	+0,515	+0,275	+0,530	+0,558	+0,293	+0,597	+0,610	+0,388	+0,545	+0,582	+0,300
7	+0,289	+0,301	+0,0980	+0,333	+0,346	+0,0964	+0,402	+0,398	+0,189	+0,357	+0,387	+0,134
8	+0,064	+0,0785	−0,0438	+0,099	+0,111	−0,0453	+0,162	+0,152	+0,019	+0,111	+0,139	−0,0218
9	−0,163	−0,128	−0,170	−0,142	−0,115	−0,183	−0,084	−0,0919	−0,131	−0,242	−0,258	−0,218
10	−0,391	−0,353	−0,317	−0,390	−0,373	−0,339	−0,344	−0,381	−0,299	−0,519	−0,487	−0,397
11	−0,532	−0,496	−0,428	−0,571	−0,570	−0,460	−0,535	−0,626	−0,428	−0,677	−0,627	−0,461
12	−0,562	−0,475	−0,512	−0,616	−0,611	−0,570	−0,600	−0,768	−0,531	−0,637	−0,624	−0,505
13	−0,541	−0,465	−0,494	−0,578	−0,574	−0,543	−0,559	−0,705	−0,475	−0,614	−0,600	−0,485
14	−0,555	−0,454	−0,538	−0,596	−0,553	−0,593	−0,559	−0,665	−0,488	−0,614	−0,540	−0,563
15	−0,558	−0,454	−0,586	−0,594	−0,567	−0,638	−0,565	−0,677	−0,523	−0,611	−0,548	−0,550
16	−0,646	−0,534	−0,921	−0,651	−0,670	−0,995	−0,594	−0,727	−0,627	−0,658	−0,675	−0,970
17	−0,672	−0,590	−0,768	−0,677	−0,801	−0,755	−0,603	−0,755	−0,613	−0,682	−0,721	−0,862
18	−0,685	−0,669	−0,638	−0,666	−0,885	−0,573	−0,603	−0,800	−0,615	−0,685	−0,813	−0,606
19	−0,709	−0,784	−0,552	−0,665	−0,941	−0,513	−0,598	−0,792	−0,627	−0,675	−0,895	−0,517
20	−0,737	−0,859	−0,490	−0,656	−0,960	−0,526	−0,592	−0,812	−0,713	−0,672	−0,937	−0,535
21	−0,755	−0,990	−0,469	−0,655	−0,920	−0,549	−0,583	−0,803	−0,972	−0,655	−0,943	−0,635
22	−0,750	−1,001	−0,467	−0,644	−0,875	−0,652	−0,568	−0,773	−1,170	−0,648	−0,894	−0,737
23	−0,734	−0,960	−0,606	−0,620	−0,874	−1,242	−0,555	−0,750	−1,095	−0,637	−0,835	−1,315
24	−0,738	−0,928	−1,805	−0,621	−0,850	−1,375	−0,554	−0,745	−1,055	−0,634	−0,838	−1,465
25	−0,728	−0,936	−1,825	−0,615	−0,854	−1,365	−0,552	−0,738	−1,031	−0,634	−0,826	−1,453
26	−0,728	−0,921	−1,800	−0,615	−0,870	−1,31	−0,548	−0,748	−1,020	−0,631	−0,937	−1,460

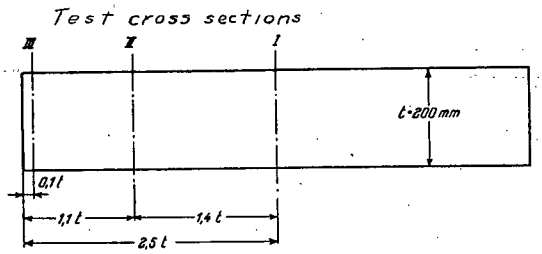

Figure 1.- Location of test sections on the NACA airfoils 2212 and M 6.

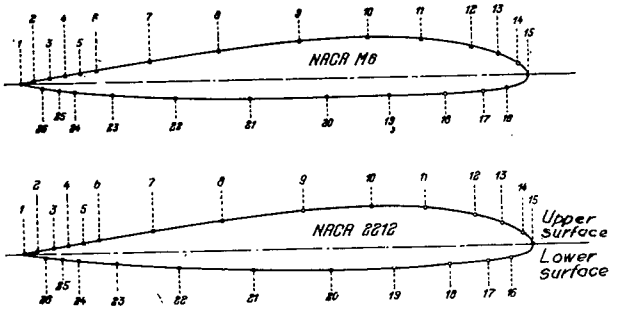

Figure 2.- Arrangement of test stations.

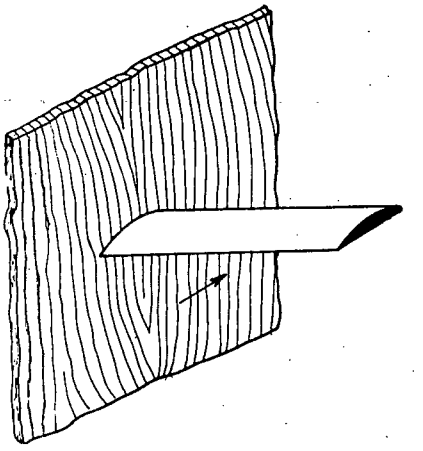

Figure 3.- Test set up for measurement in section III.

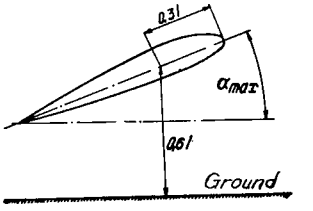

Figure 4.

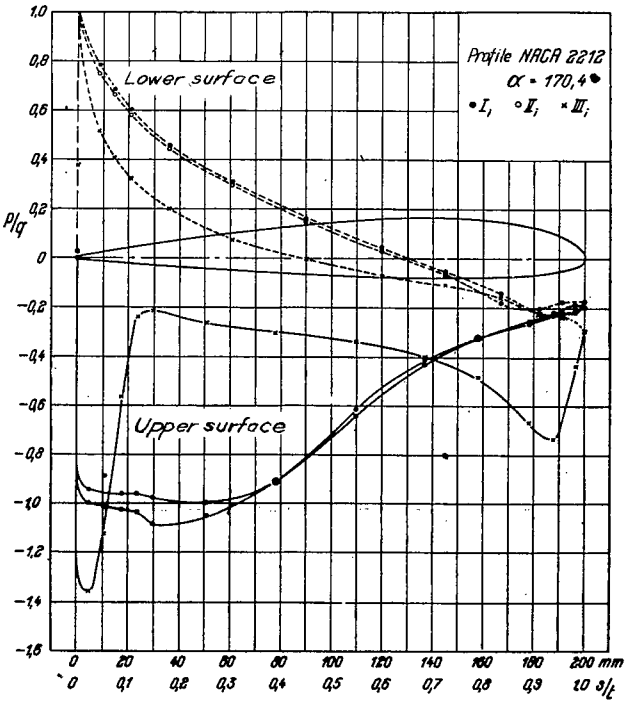

Figure 5.

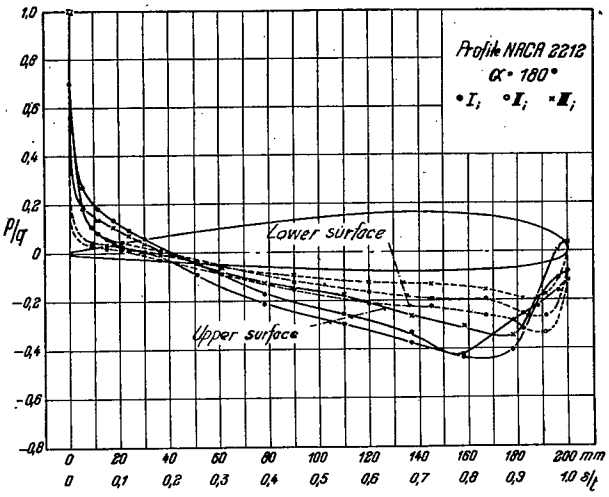

Figure 6

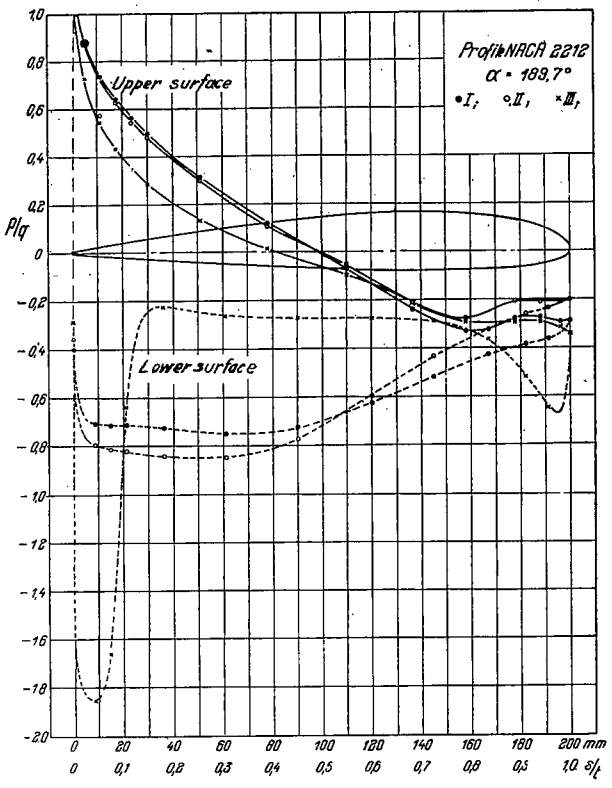

Figure 7.

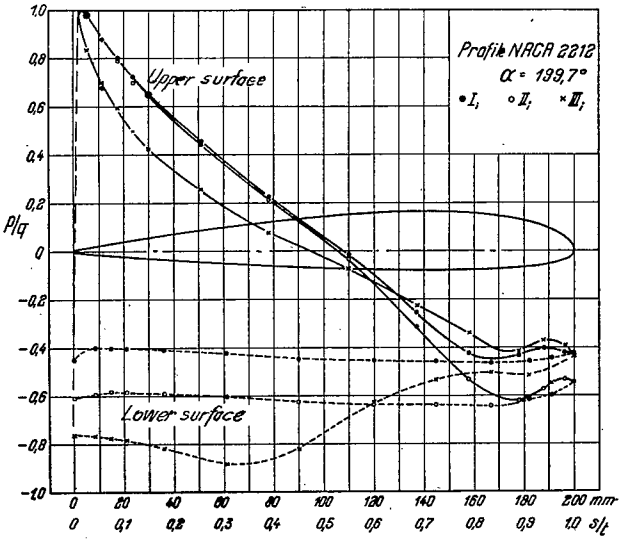

Figure 8.

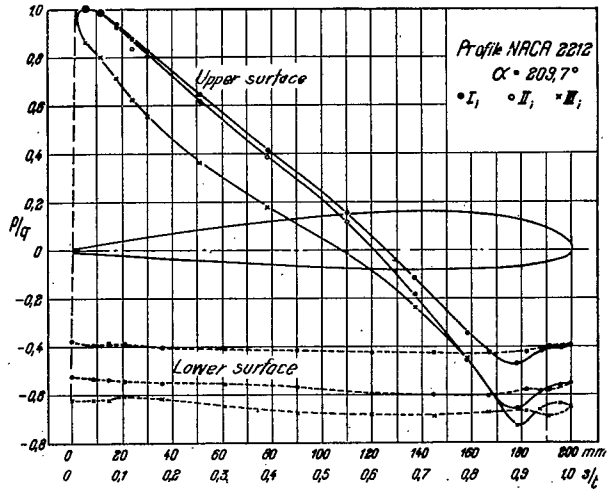

Figure 9.

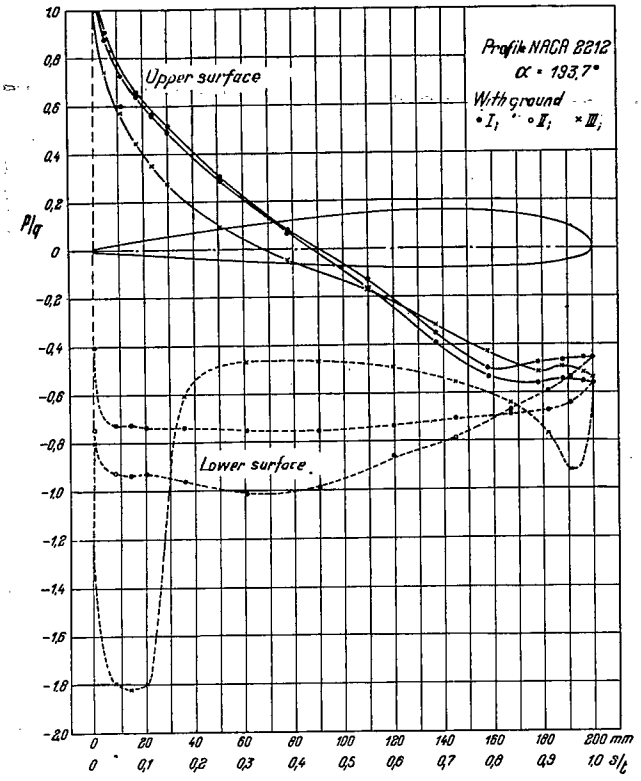

Figure 10.

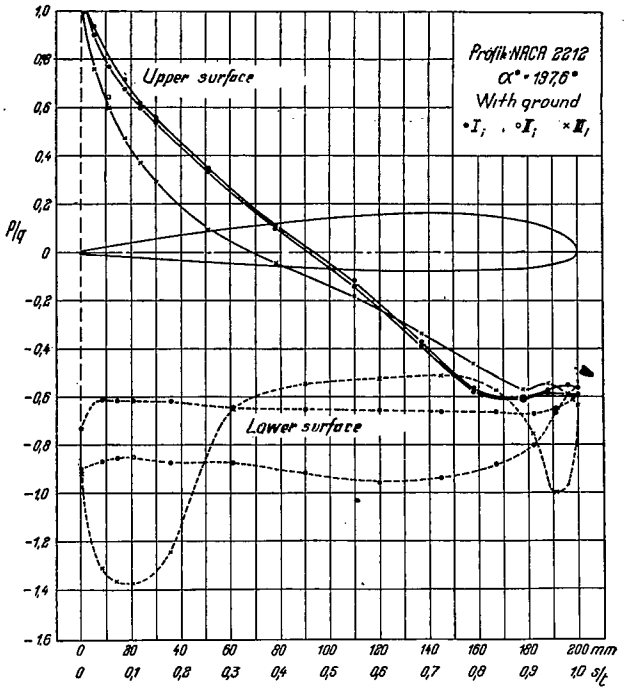

Figure 11.

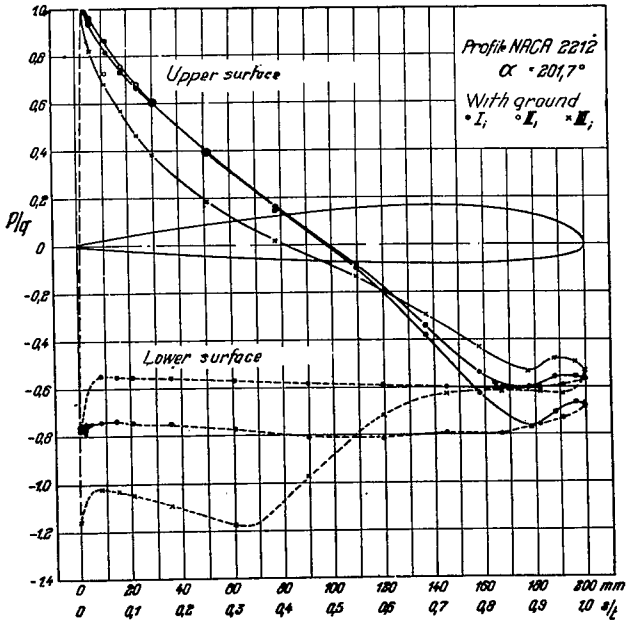

Figure 12.

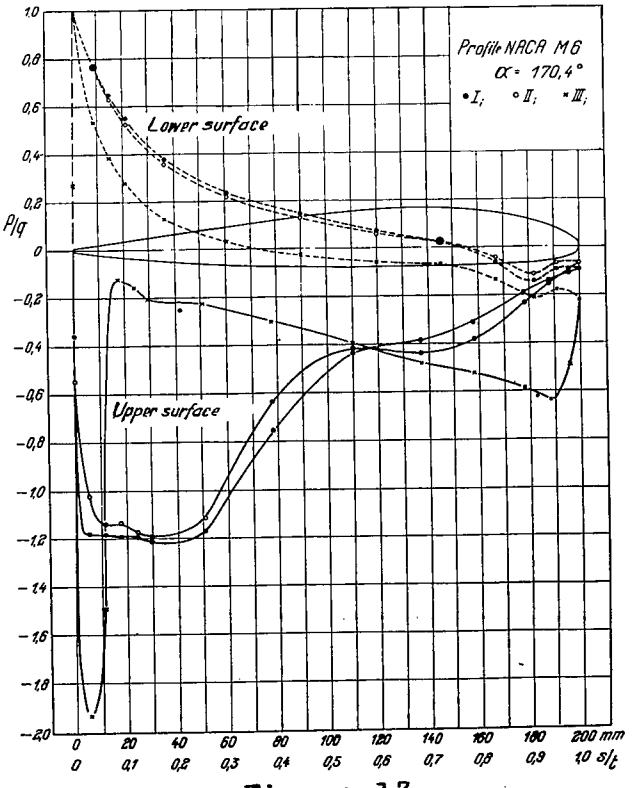

Figure 13.

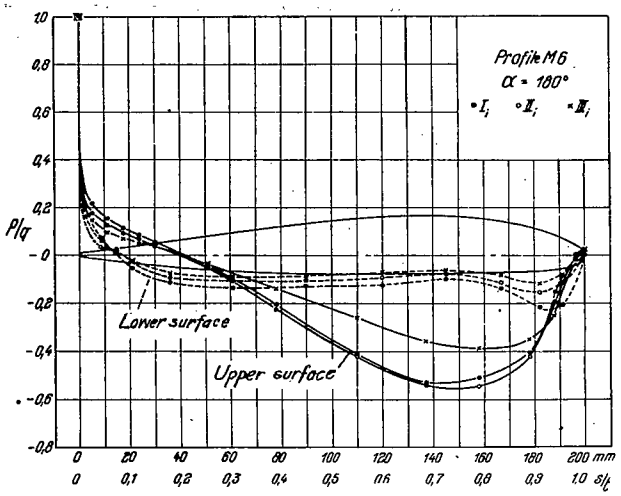

Figure 14.

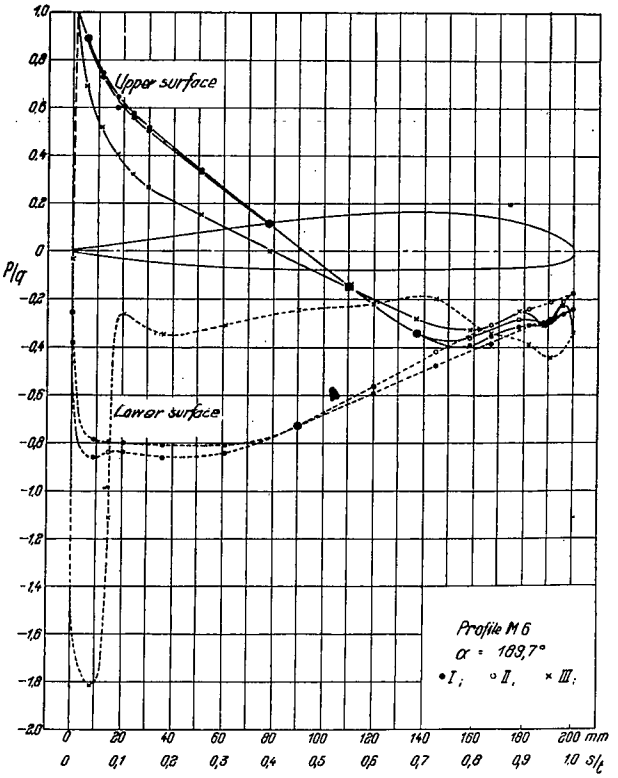

Figure 15.

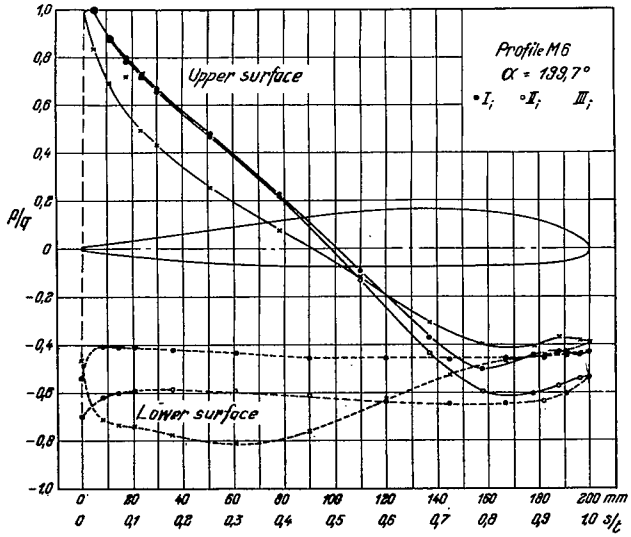

Figure 16.

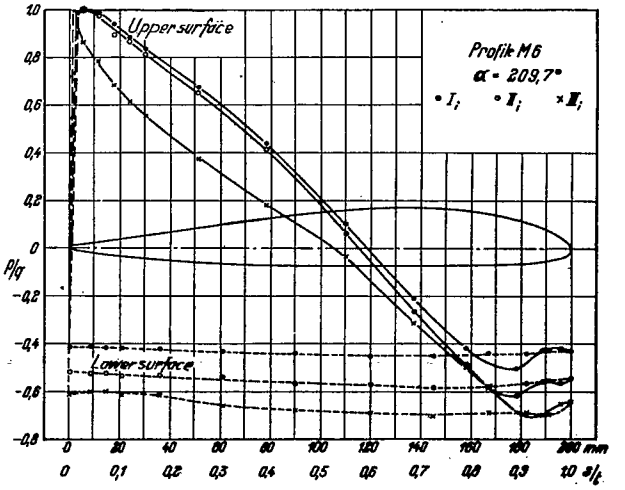

Figure 17.

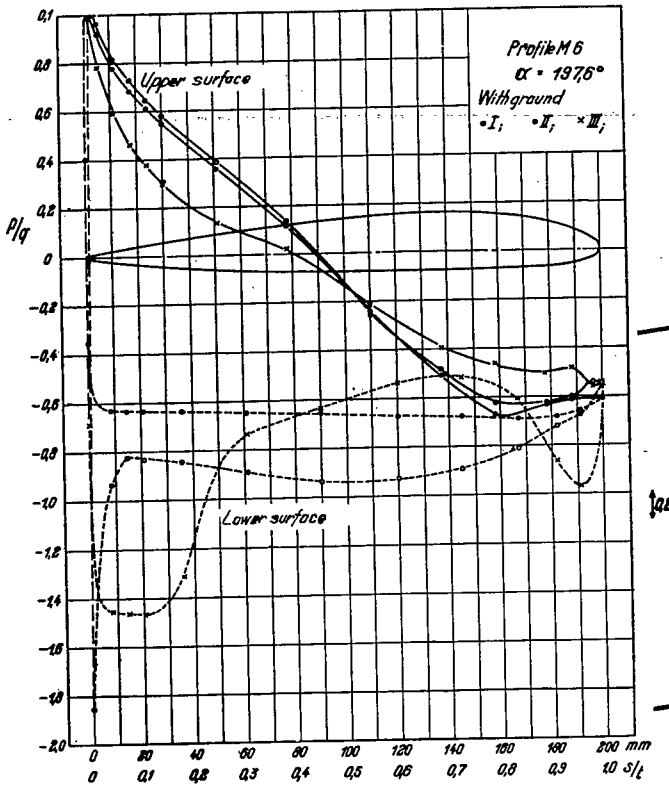

Figure 18.

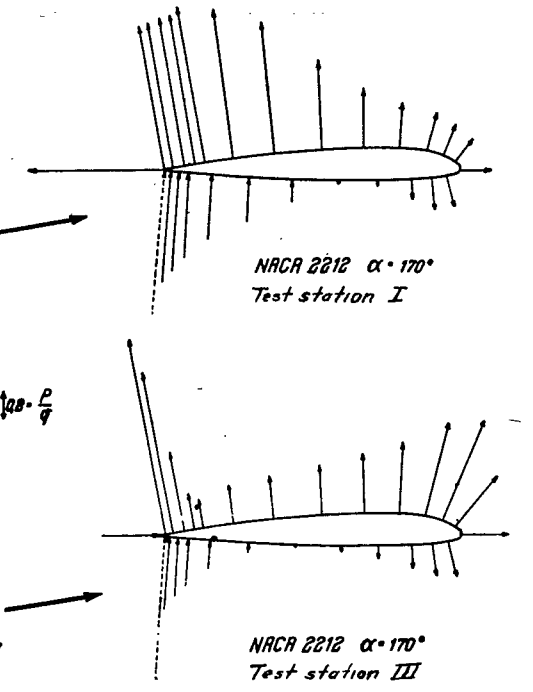

Figure 19.- Pressure distribution for $\alpha = 170.4^{\circ}$ (NACA airfoil 2212).

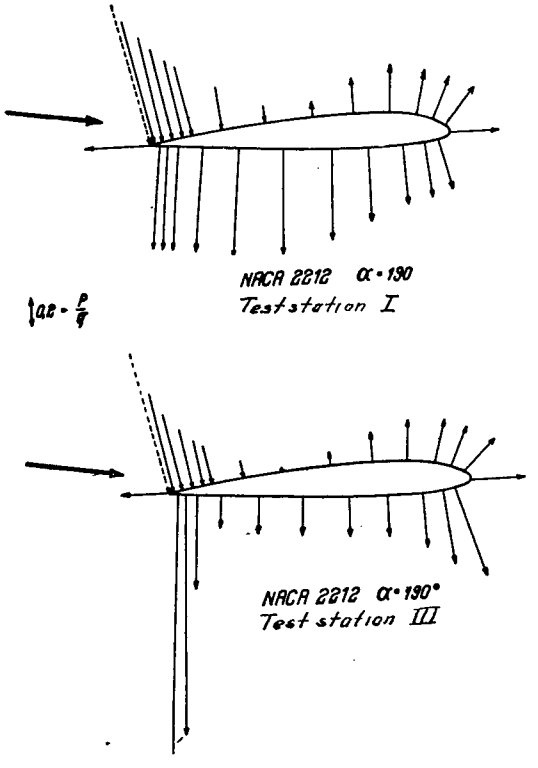

Figure 20.- Pressure distribution for $\alpha = 189.6^{\circ}$ (NACA airfoil 2212).

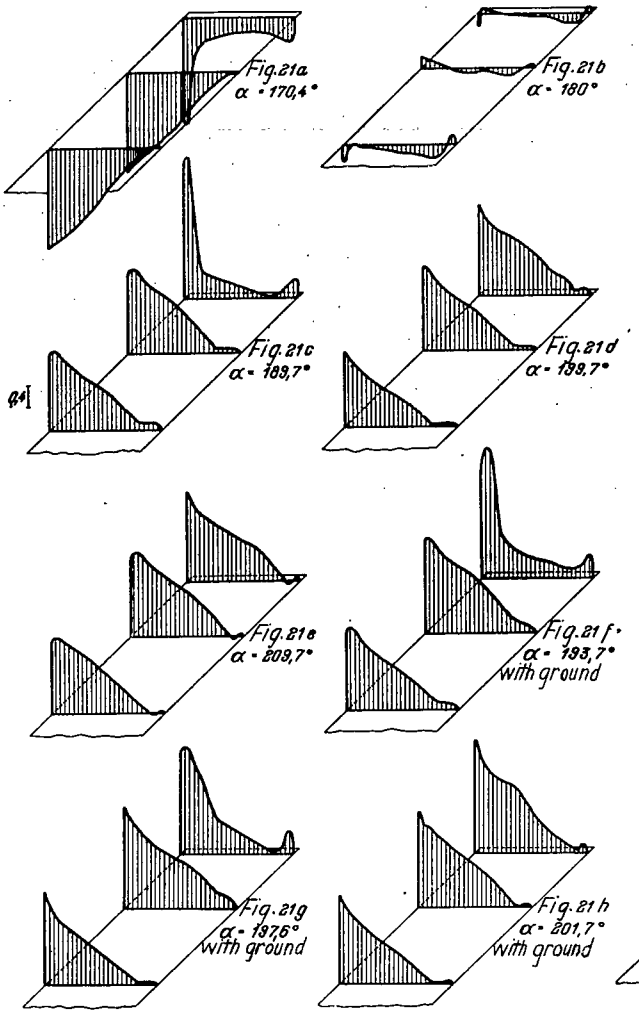

Figure 21.- Load distribution (NACA airfoil 2212).

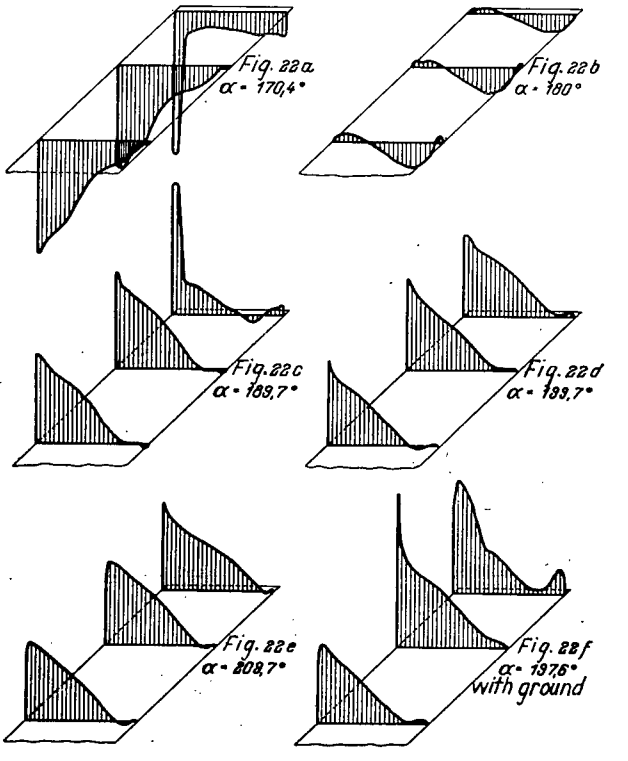

Figure 22.- Load distribution (NACA airfoil M 6).

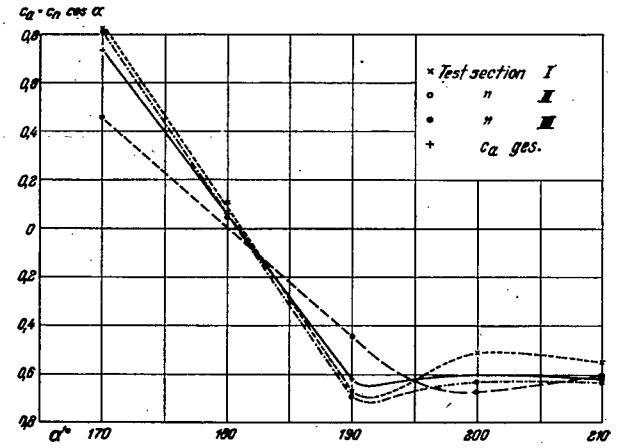

Figure 24.- C_a versus angle of attack (NACA airfoil 2212).

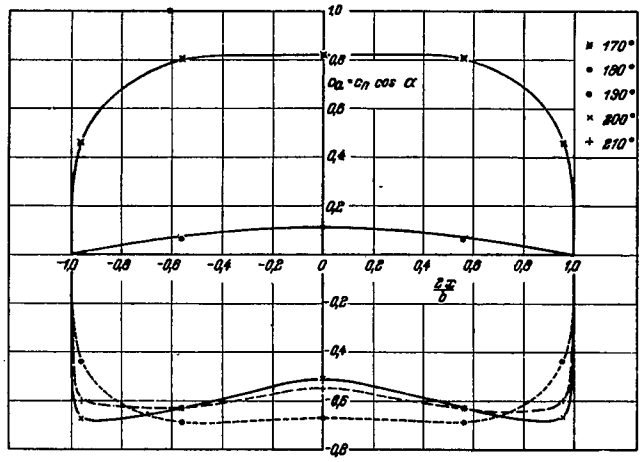

Figure 23.- Spanwise load distribution (NACA airfoil 2212).

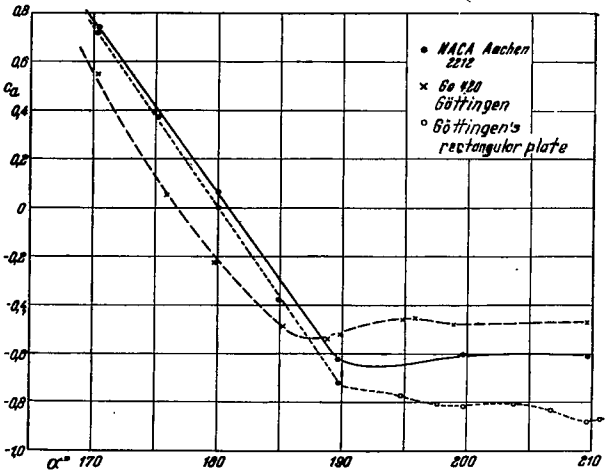

Figure 25.- Comparison of C_a values for NACA airfoil 2212, Gö 420 and a flat rectangular plate.

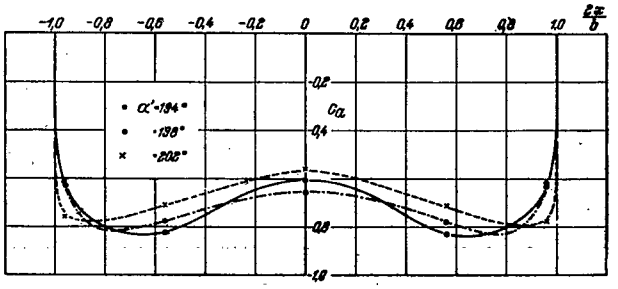

Figure 26.- Spanwise load distribution in ground proximity (NACA airfoil 2212).

DO NOT REMOVE SLIP FROM MATERIAL

Delete your name from this slip when returning material to the library.

NAME	MS
~~K. Dotton~~	~~167~~
Dennis Petley 3/16/95	350

NASA Langley (Rev. May 1988) RIAD N-75